JGR Atmospheres

Key Points:

- Substantial interannual variability in monthly mean amplitudes of the 12-hr tide above Rothera is characterized
- The climate indices F10.7, QBO10, QBO30, and SAM display significant correlations with interannual variability of 12-hr tidal amplitudes
- El Niño Southern Oscillation does not show a significant correlation to the 12-hr tidal amplitudes over Rothera, suggesting no linear link

Interannual Variability of the 12-hr Tide in the Mesosphere and Lower Thermosphere in 15 Years of Meteor-Radar Observations Over Rothera (68°S, 68°W)

Shaun M. Dempsey[1,2] , **Phoebe E. Noble**[1,2] , **Corwin J. Wright**[1] , **Nicholas J. Mitchell**[1,2] , and **Tracy Moffat-Griffin**[2]

[1]Department of Electronic and Electrical Engineering, Centre for Atmospheric and Oceanic Sciences, University of Bath, Bath, UK, [2]British Antarctic Survey, Cambridge, UK

Abstract The solar tides of the mesosphere and lower thermosphere (MLT) show great variability on time scales of days to years, with significant variability at interannual time scales. However, the nature and causes of this variability remain poorly understood. Here, we present measurements made over the interval 2005–2020 of the interannual variability of the 12-hr tide as measured at heights of 80–100 km by a meteor radar over Rothera (68°S, 68°W). We use a linear regression analysis to investigate correlations between the 12-hr tidal amplitudes and several climate indices, specifically the solar cycle (as measured by F10.7 solar flux), El Niño Southern Oscillation (ENSO), the Quasi-Biennial Oscillation (QBO) at 10 and 30 hPa and the Southern Annular Mode (SAM). Our observations reveal that the 12-hr tide has a large amplitude and a clearly defined seasonal cycle with monthly mean values as large as 35 m s^{-1}. We observe substantial interannual variability, with monthly mean 12-hr tidal amplitudes at 95 km exhibiting a two standard-deviation range (2σ) in spring of 13.4 m s^{-1}, 11.2 m s^{-1} in summer, 18.6 m s^{-1} in autumn, and 7.0 m s^{-1} in winter. We find that F10.7, QBO10, QBO30, and SAM all have significant correlations to the 12-hr tidal amplitudes at the 95% level, with a linear trend also present. Whereas we detect very minimal correlation with ENSO. These results suggest that variations in F10.7, the QBO and SAM may contribute significantly to the interannual variability of 12-hr tidal amplitudes in the Antarctic MLT.

1. Introduction

In the mesosphere and lower thermosphere (MLT), at heights of 80–100 km, the wind field is dominated by the global scale oscillations of the solar atmospheric tides. These tides can reach very large amplitudes of several 10s of m s^{-1} and can be critical to the dynamics and coupling of the whole atmosphere. These tides are primarily excited by the solar heating of ozone and water vapor in the stratosphere and troposphere, the release of latent heat in deep tropospheric convection, and/or nonlinear interactions involving tides and planetary waves (Hagan & Forbes, 2002; Vadas et al., 2014).

The tides are apparent in many different atmospheric variables, including wind, temperature, and density. They are often the most prominent features of the wind field of the MLT. Consequently, they can profoundly impact the coupling and dynamics of the atmosphere. For example, tidal winds can filter the field of atmospheric gravity waves (Beldon & Mitchell, 2010). This filtering controls the propagation of gravity waves to greater heights, thus modulating gravity-wave momentum fluxes and the resulting forcing of the global atmospheric circulation (Fritts & Alexander, 2003; Yiğit et al., 2021). In addition to wind perturbations, tidal temperature perturbations can also play an important role and are thought to be a driver of the variability of polar mesospheric clouds, modulating the cloud ice crystal population (Fiedler et al., 2005).

Tides can propagate upwards from the MLT, higher into the upper thermosphere, where they may affect neutral and plasma concentrations in the ionosphere's E and F regions, modulating the ionospheric wind dynamo (Liu, 2016; Sobhkhiz-Miandehi et al., 2022; Yiğit & Medvedev, 2015). These important features mean that understanding the tides is vital to understanding the dynamics and coupling of atmospheric layers (Smith, 2012).

Observations of MLT winds reveal large amplitude tides with periods which are harmonics of the solar day (Chapman & Lindzen, 1970). At middle and polar latitudes, the largest amplitudes are observed in the 12-hr tide, with the 24-hr and 8-hr tides having significantly smaller amplitudes (Davis et al., 2013; Dempsey et al., 2021). The dominance of the 12-hr tide at polar latitudes means that determining the climatology and variability of

Software: Shaun M. Dempsey, Phoebe E. Noble
Supervision: Corwin J. Wright, Nicholas J. Mitchell, Tracy Moffat-Griffin
Validation: Phoebe E. Noble, Corwin J. Wright
Writing – original draft: Shaun M. Dempsey
Writing – review & editing: Shaun M. Dempsey, Phoebe E. Noble, Corwin J. Wright, Nicholas J. Mitchell, Tracy Moffat-Griffin

this tide is particularly important in studies of the polar atmosphere. Consequently, a number of observational studies have attempted to determine the climatology and variability of the 12-hr tide at polar latitudes, including Mitchell (2002), Conte et al. (2017), and Dempsey et al. (2021). Here, our focus is on the 12-hr tide alone, and we will not further consider the 24-hr or 8-hr tides.

The polar 12-hr tide in the MLT is known to display a distinct seasonal variability with maximum amplitudes generally occurring at heights above 90 km in the autumn months of April-May (in the case of Rothera in the Southern Hemisphere), with a secondary maximum occurring at similar heights in August-September (Dempsey et al., 2021; Mitchell, 2002). Beyond this, the polar 12-hr tide is also observed to display significant interannual variability with changes in amplitude of several m s^{-1} occurring from year to year (Conte et al., 2017). These latter variations in amplitude have been proposed to be linked to external drivers that modify the tide's excitation and/or propagation. Potential drivers of interannual variability at polar and other latitudes include:

1. solar variability (e.g., Beldon et al., 2006; Bremer et al., 1997; Guharay et al., 2019; Namboothiri et al., 1993; Nischal et al., 2019),
2. the El Niño Southern Oscillation (ENSO) (e.g., Lieberman et al., 2007; Liu et al., 2017; Pedatella & Liu, 2012; Sundararajan, 2020, amongst others),
3. and the stratospheric Quasi-Biennial Oscillation (QBO) (e.g., Forbes et al., 2008; Hibbins et al., 2007, 2010; Laskar et al., 2016; Pancheva et al., 2009).

We should also note that in addition to this interannual variability, the 12-hr tide displays great short-term variability on time scales ranging from a few days to several months. In addition, short-term tides also respond to the QBO, ENSO, and solar cycle (see Dhadly et al., 2018; Kumari & Oberheide, 2020; Vitharana et al., 2019). Here, however, we will consider only the interannual variability.

We will now consider the above potential drivers of interannual variability in the polar 12-hr tide in more detail.

Variations in solar flux are an obvious potential driver of variability because the migrating component of tides is strongly excited by the solar heating of ozone and water vapor in the troposphere and stratosphere and the temperature structure of the atmosphere through which the tide must propagate may similarly change. A negative correlation between F10.7 solar flux and tidal amplitudes has been reported by Sprenger and Schminder (1969), Namboothiri et al. (1993), and Bremer et al. (1997). At polar latitudes, Baumgaertner et al. (2005) investigated the relationship between solar flux and Antarctic 12-hr tidal amplitudes measured at Scott Base (78°S, 167°E) using an MF radar and discovered a negative correlation between solar F10.7 flux and tidal amplitudes. These authors also noted a positive trend in tidal amplitudes, which they suggested might be a consequence of increased cooling of the atmosphere produced by a rise in CO_2 resulting in pressure and density decreases in the MLT. This would increase tidal amplitudes at a particular height, given that the gas density at this height would be decreased.

ENSO causes large-scale changes in tropospheric convection (Lieberman et al., 2007; Trenberth, 2002). These changes may modify tidal forcing in the troposphere, resulting in corresponding tidal variability in the MLT. Zonal mean winds in the stratosphere and mesosphere are also believed to be influenced by ENSO (Sassi, 2004) and thus may modulate tidal amplitudes in the global MLT by changing the propagation environment for the tide (Pedatella & Liu, 2012).

QBO signatures have been found in 12-hr MLT tides in a number of studies. For example, at midlatitudes, Forbes et al. (2008) found QBO modulations of $\pm10\%$–15% in 12-hr tidal amplitudes. They proposed that this was due to modulation by the QBO as the tides propagate upwards from their tropospheric and stratospheric source regions into the MLT. Pancheva et al. (2009) investigated temperature tides using data from Sounding of the Atmosphere using Broadband Emission Radiometry (SABER) and winds from the TIMED Doppler Interferometer (TIDI) onboard the Thermosphere Ionosphere Mesosphere Energetics and Dynamics (TIMED) satellite and reported QBO modulation of the migrating 12-hr tidal amplitude at midlatitudes in both hemispheres. At polar latitudes, Hibbins et al. (2007, 2010) used the SuperDARN radar located at Halley, Antarctica (76°S, 27°W) to measure meteor winds in both the zonal and meridional components and observed a large QBO modulation of the summertime 12-hr nonmigrating tide. Laskar et al. (2016) investigated the 12-hr tide at 69°N, a conjugate latitude to our study, using meteor-radar observations and Modern Era-Retrospective Analysis for Research and Applications (MERRA) winds and reported that variations in the enhancement of the tidal amplitudes during August to September are linked to low-latitude QBO winds.

The Southern Annular Mode (SAM) describes the north/south movement of the belt of eastward winds centered at 50/55° latitude (Marshall, 2003). It substantially impacts the climatic systems of the southern hemisphere's high and midlatitudes and influences climate variability and change in the southern hemisphere. The surface zonal winds of SAM and the southern hemisphere greatly impact the tropospheric and oceanic circulation systems (Abram et al., 2014; Lee et al., 2019). However, there have been very few studies of the links between the SAM and MLT winds and tides. Merzlyakov et al. (2009) investigated MLT wind and tide measurements from a meteor radar situated at Molodezhnaya (67.7°S, 45.9°E) and MF radars at Mawson (67.6°S, 62.9°E) and Davis (68.6°S, 78.0°E). They found no significant link between SAM and the MLT. In contrast, Noble et al. (2022) found a correlation between the SAM and MLT winds measured by meteor radar at Rothera in the same data set as considered in our study. It is possible that the SAM modulation of MLT winds could impact MLT tidal amplitudes.

In this study, we use meteor-radar observations of zonal and meridional winds in the Antarctic MLT made at Rothera (68°S, 68°W) to measure the amplitude of the 12-hr tide. We determine its seasonal variability and its interannual variability. We then use a linear regression model to identify any correlations between the interannual variability of monthly estimates of tidal amplitude and indices representing climate processes. The model includes terms that represent the following potential drivers of tidal variability:

1. solar variability as measured by the F10.7 solar flux,
2. the El Nino Southern Oscillation (ENSO),
3. the Quasi-Biennial Oscillation (QBO),
4. the Southern Annular Mode (SAM).

The meteor radar at Rothera is an ideal instrument for this type of study because it is able to make robust measurements of tidal amplitude at heights of 80–100 km over extended intervals. Here, we use observations made over the interval 2005–2020, forming one of the longest records of polar MLT winds available.

In Section 2, we describe the radar, data and climate indices we have used. Section 3 describes the methods used to obtain estimates of monthly tidal amplitudes from hourly winds and the linear regression analysis used to extract the time series correlation of the tidal amplitudes and the climate indices. In Section 4, we present the results of our analysis. In Section 5, we consider our results compared to other studies linking tidal amplitudes in the MLT and climate indices. Finally, in Section 6, we present our conclusions.

2. Data

2.1. Meteor Radar

Meteor radars have been used in many ground-based tidal studies (e.g., Beldon et al., 2006; Davis et al., 2013; Dempsey et al., 2021; Mitchell, 2002; Stober, Kuchar et al., 2021) and are a well-established method of measuring MLT winds from 75 to 105 km. Using inferred winds from meteor trails, meteor radars can determine tidal amplitudes, wavelengths, and variability at various scales. They are able to measure small-scale gravity waves with periods of <2 hr, with horizontal wavelengths <400 km and vertical wavelengths up to 3–5 km (Song et al., 2021). The radars have also been used to investigate planetary waves, such as the interaction between the 12-hr tide and the 16-day planetary wave (Day et al., 2012; Mthembu et al., 2013). They are ideally suited to investigating MLT tidal amplitudes, which become large at these heights. As such, meteor radars are well-suited to study interannual tidal variability.

We are using tidal amplitudes obtained from hourly winds measured in the MLT by a SKiYMET VHF meteor radar located at Rothera (68°S, 68°W) from 1 January 2005 to 31 December 2020. Hourly winds are estimated using the radial velocity measurements taken from each individual meteor, assuming that the flow is horizontal and uniform across the meteor collecting volume at any given height. We calculate the winds by combining the inferred horizontal velocities obtained for each meteor with a Gaussian weighting in height and time around a specific height and specific time. The full-width-half-maxima for these Gaussian weightings are 2 hr in time and 3 km in height. The center of the Gaussian progresses across the data in 1-hr time and 1-km height steps, giving hourly winds between 75 and 105 km (Hindley et al., 2021).

The Rothera radar employs a solid-state transmitter with a peak power of 6 kW and was installed in 2005. In 2019, the antennae were replaced following weather-related degradation. This reduced the fraction of ambiguous meteors detected. The radar antenna receiver array uses five interferometer elements to measure echo azimuth

and zenith angles. When combined with range data, the height of individual meteor echoes can be determined (Mitchell & Beldon, 2009). In practice, this allows us to determine MLT winds down to ∼2 hr in time and 2 km in space. However, as we step the Gaussian weightings by 1 hr in time and 1 km in height, we are able to use hourly winds in calculations. The meteor radar installed at Rothera (68°S, 68°W) has been used in numerous studies for investigating MLT winds (Sandford et al., 2010), atmospheric tides (Beldon & Mitchell, 2010; Dempsey et al., 2021; Sandford et al., 2007), planetary waves (Mthembu et al., 2013), and gravity waves (Beldon & Mitchell, 2009; Mitchell & Beldon, 2009).

For a detailed overview of the Rothera meteor radar, see Mitchell and Beldon (2009). Note, as we only use one radar in this study, we are unable to separate migrating (sun-following, westward propagating) and nonmigrating modes (not sun-following) and observe a superposition of both. For a detailed description of general SKiYMET radar operation, see Hocking et al. (2001). Due to an increased spread of meteor height distribution at certain periods over the data set, the following days have been removed: January 2005, December 2009, January 2010, December 2010, and the entirety of 2016–2018.

2.2. Time Series of Climate Indices

To qualify the dependence of tidal amplitudes on specific climate indices, we regress monthly values of five climate indices and time against 12-hr tidal amplitudes. These indices are F10.7 solar flux, ENSO, QBO10, QBO30, and SAM.

For solar flux, we use the observed solar flux F10.7 index, defined as the solar radio flux at 10.7 cm radio emission measured on the surface of Earth. It is one of the longest-running records of solar activity, so we can use it as an indicator of solar activity in our linear regression. It is measured in solar flux units (SFU), with 1 SFU equal to 10^{-22} W m^{-2} Hz^{-1} and provided by the National Research Council of Canada.

For the ENSO, we use the Niño 3.4 index, representing the average equatorial sea surface temperature (SST) anomalies (measured in kelvin) in a box bound by 5°N–5°S, 170°W–120°W. This index uses a 5-month running mean, and the El Niño or La Niña events are defined when the Niño 3.4 SST anomalies exceed ±0.4 K for 6 months or more (Trenberth, 2018).

For the QBO indices, the ERA5 zonal mean zonal wind (in m s^{-1}) is averaged over 5°N–5°S at 10 hPa for the QBO10 index and at 30 hPa for the QBO30 index. These two heights were chosen to capture possible QBO responses because they are almost orthogonal to each other (Chiodo et al., 2014; see Figure S1 in Supporting Information S1). Using both indices gives more opportunity to find any linear connections compared to using just one.

For the SAM, we use the Marshall Southern Annular Mode index (SAM index), which is the difference between the normalized monthly zonal sea level pressure (SLP) at 40°S minus the normalized monthly zonal SLP at 65°S. Six stations are used to calculate a proxy zonal mean SLP at both 40°S and 65°S (Marshall, 2003, 2018).

Figure 1 presents the time series of the five climate indices over the 2005–2020 period. Our chosen period encompasses the entirety of solar cycle 24, which has a minimum in December 2008 and the following minimum in December 2019, shown in Figure 1a. In Figure 1b, the ENSO index varies systematically from 25 to 29 K but without a strongly fixed period. The QBO10 index in Figure 1c has a more defined period, with a regular period of around 22 months. This is similar to the QBO30 (in Figure 1d) index, which has a similar period but lagged by around 9 months from the QBO10 index (for a Lomb-Scargle periodogram of these two indices, please see Figure S2 in Supporting Information S1). Finally, in Figure 1e, the SAM index does not have a strong periodicity and no apparent trend.

2.2.1. Inclusion of an Ozone Term

One driver for atmospheric tides is the solar excitation of ozone in the stratosphere. It would therefore make sense to use an index representing ozone in our linear regression. However, the inclusion of this term in our model would cause it to be unstable due to correlations with ENSO and also time, i.e., the presence of a linear trend (for a complete table of the correlation of the climate indices against the other indices used in the study, please see Table S1 in Supporting Information S1). Therefore, we have decided to omit the ozone term to investigate any potential links with ENSO. This is consistent with Pancheva et al. (2003) who found that ozone can be used as
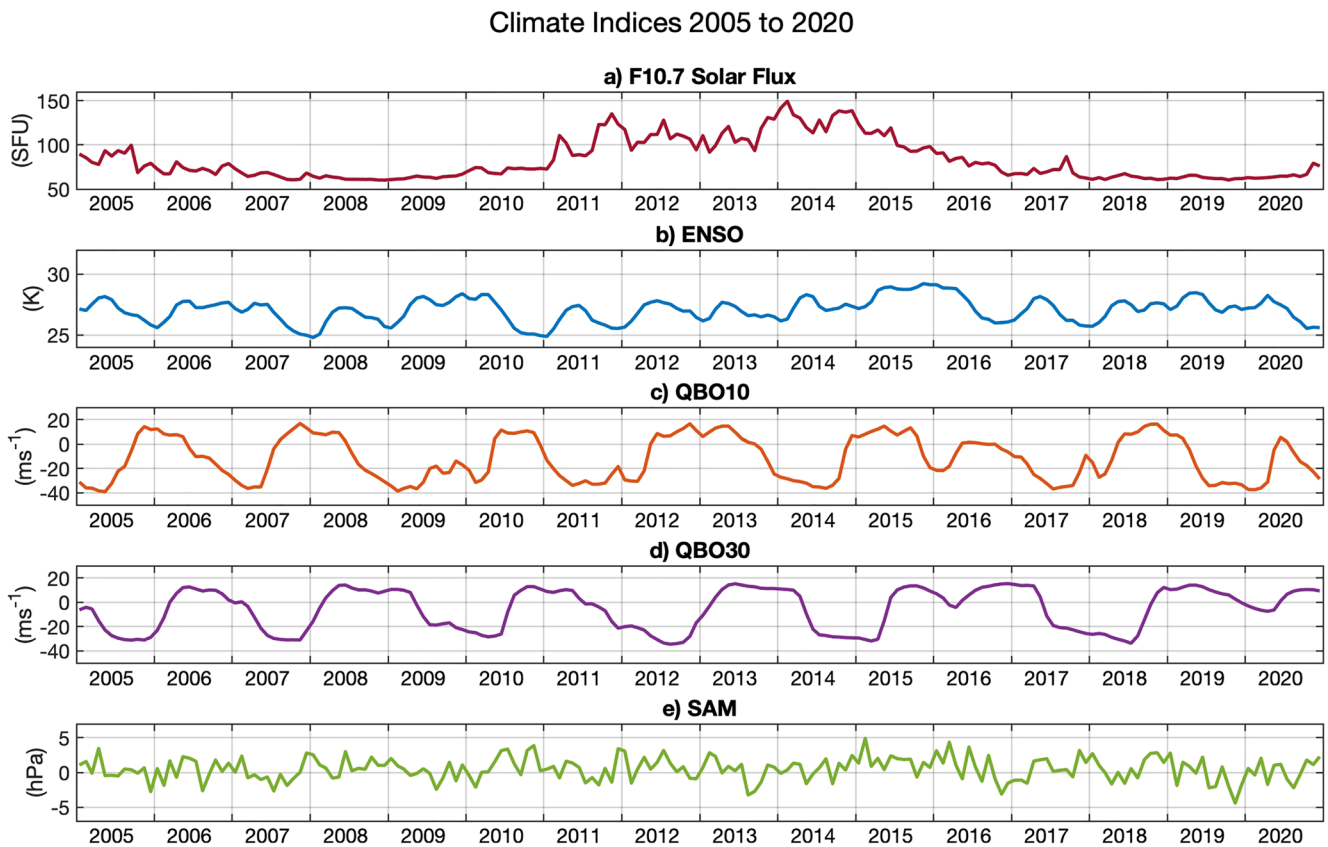
Figure 1. Time series of the global climate indices of (a) F10.7 solar flux, (b) ENSO, (c) QBO10, (d) QBO30, and (e) SAM for the period 2005–2020.

a proxy for planetary wave activity. As we are considering an absorption term with the inclusion of F10.7 solar flux, we are not proceeding with any ozone term in our linear model.

3. Method

3.1. Tidal Amplitudes From Hourly Winds

To investigate the interannual variability of the tides in the MLT, we calculate amplitudes of the 12-hr tide using meteor radar hourly winds over the time period 2005–2020. We obtain tidal amplitudes by creating a monthly composite day of the winds and fitting sinusoidal waves of tidal periods to the composite day at each height. These have periods of 24, 12, 8, and 6 hr. For more detail, see Dempsey et al. (2021). We will be using only the 12-hr tide for this study, as this tide has the largest amplitude at this latitude.

3.2. Linear Regression

We will now explain our linear regression analysis of the 12-hr tidal amplitudes. Similarly to Gan et al. (2017) and Ramesh et al. (2020), we begin with the tidal anomaly. This is defined as the deviation of each month from the climatological mean. This step is to remove the seasonal cycle.

To build a multilinear regression model for each month, we separate our data and use a 3-month window centered on the month of interest. The linear regression analysis is performed independently on each height level for the meridional and zonal tidal amplitudes. We propose and implement the following linear regression model and estimate the unknown parameters using the Ordinary Least Squares (OLS) method. We use the following expression for the linear model:

$$A'_{12} = \beta_0 + (\beta_1 F10.7) + (\beta_2 ENSO) + (\beta_3 QBO10) + (\beta_4 QBO30) + (\beta_5 SAM) + (\beta_6 Time) \tag{1}$$

where A'_{12} is the 12-hr tidal amplitude minus the seasonality, β_0 is the constant, and β_1 to β_6 are the coefficients of the climate variables.

Linear regression is a robust technique for finding correlations between variables, and it allows us to deconstruct the tidal anomaly into component portions that can be attributed to various external factors. However, correlation does not always imply causality; hence, a correlation between tidal amplitudes and indices could be purely coincidental rather than causal. There are likely to be other causes of interannual variability besides the indices we regress against, but it is impossible to include everything without overcomplicating our model. Therefore, we must interpret the results with caution when employing linear regression. Treated carefully, these findings allow us to investigate linear impacts of atmospheric and solar oscillations on tidal amplitudes in the Antarctic MLT.

3.2.1. Multicollinearity

For the linear regression to be valid, we need to check that there is no multicollinearity, i.e., that none of the indices used are correlated with each other. The presence of multicollinearity means variables is correlated. If that were the case, then the results from our linear regression would be unreliable. This test ensures that solar flux, ENSO, QBO10, QBO30, SAM, and time are independent. We test this by calculating Variance Inflation Factors (VIFs).

VIFs are created by first regressing each independent variable against the others and then calculating the VIF as follows:

$$VIF = \frac{1}{(1 - R^2)} \tag{2}$$

where R^2 is the R-squared value. The values of the VIF range from 1 to infinity, with values around 1 suggesting that there is no multicollinearity; values between 1 and 5 suggesting some multicollinearity, but not enough to disrupt the model; values over 5 suggesting correlation and are cause for concern; and values over 10 are a major problem and imply a strong correlation (Kalnins, 2018). For our linear regression, the VIFs range from 1.02 to 1.35. As our values are around 1, the variables we have chosen to explain tidal amplitude variability do not suffer from multicollinearity, and therefore, we can use them confidently.

3.2.2. Autocorrelation

To perform a linear regression, the residuals must be free from autocorrelation, which means the residuals from the linear regression are not correlated with each other. Autocorrelation would indicate that essential information is missing from the model and that we cannot rely on the standard errors.

To determine the presence of autocorrelation, we use the Durbin-Watson (DW) test which yields a test statistic to detect autocorrelation in the residuals from a regression analysis. It returns a number between 0 and 4 (Webster, 2012). A score of 2 indicates no autocorrelation, whereas results closer to 0 indicate positive autocorrelation, and results closer to four indicate negative autocorrelation. In the current study, we use the definition that readings between 1.5 and 2.5 are normal and results below 1 and above 3 indicate some form of autocorrelation (Webster, 2012).

Because we create a model to describe the tidal amplitudes of each month, we have many DW statistics. The meteor radar tidal amplitude DW statistics all lie in the acceptable 1–3 range, with 86% falling in the 1.5–2.5 acceptable range. Therefore, our DW results all fall within the acceptable range.

4. Results

4.1. Twelve-Hour Tidal Amplitudes

Figure 2 presents the zonal and meridional tidal amplitudes at 95 and 90 km from 2005 to 2020. In Figures 2a–2d, each pixel represents the monthly tidal amplitude given by the year on the y-axis with the month given on the x-axis. All of these plots have the same scale for comparison to each other. In Figures 2e–2h, line plots of the mean amplitude over the year with the interquartile range of the monthly amplitudes are plotted in purple and the extreme values in gray shading.
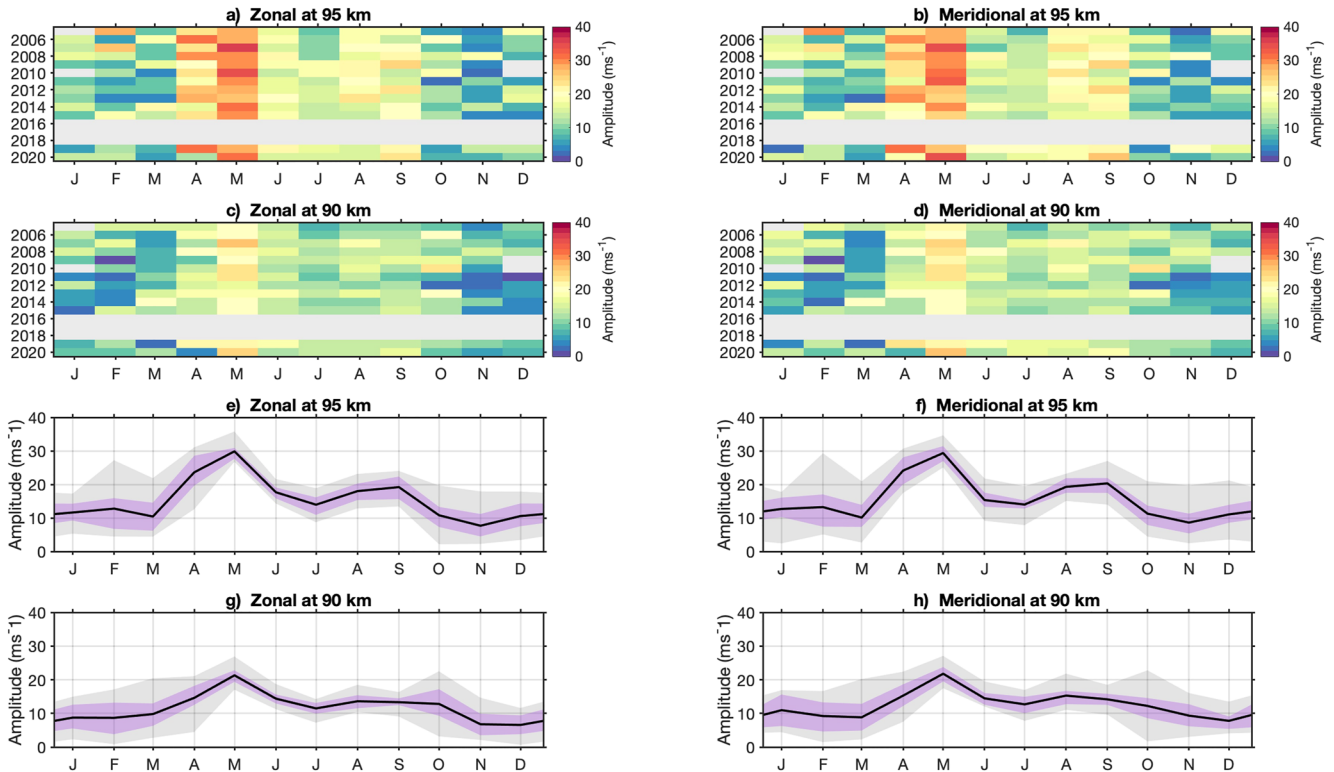
Figure 2. Monthly 12-hr tidal amplitudes for the period 2005–2020 for (a) zonal tidal amplitudes at 95 km, (b) meridional tidal amplitudes at 95 km, (c) zonal tidal amplitudes at 90 km, (d) meridional tidal amplitudes at 90 km, where each colored pixel represents the monthly tidal amplitude. The gray bars indicate where data have been removed due to quality issues. The line plots represent the average monthly tidal amplitudes, with the interquartile range of each month in purple shading and the extreme values in gray for the (e) zonal monthly 12-hr tidal amplitudes at 95 km, (f) meridional at 95 km, (g) zonal at 90 km, and (h) meridional at 90 km.

In each panel, there is considerable interannual variability. Each month exhibits a range of amplitudes from 2005 to 2020. For example, at 90 km, the month of May typically has the largest amplitudes in each year and exhibits a substantial variability in measured amplitude across the years. Similarly at 95 km, the month of May has the largest amplitudes, reaching 35 m s^{-1}, seen in Figures 2a and 2b. In panels a and b, every month exhibits considerable variability between years. For 95 km, the 2σ range in monthly mean 12-hr tidal amplitudes is 13.4 m s^{-1} in spring, 11.2 m s^{-1} in summer, 18.6 m s^{-1} in autumn, and 7.0 m s^{-1} in winter. At 90 km, in Figure 2c, we can see May 2007 exhibits an amplitude of 27 m s^{-1}, whereas in 2012, the month of May exhibits an amplitude of 15 m s^{-1}. In Figures 2c and 2d, we can see that in December (during austral summer) at 90 km, there is a large decrease in amplitudes from 2011 to 2015. At 95 km, in Figures 2a and 2b, this is not repeated. In Figures 2e–2h, we present line plots indicating the mean average of tidal amplitudes across the year with the interquartile range in purple and the extreme values in gray. We can see from these plots that, especially at 95 km, the tidal amplitudes demonstrate considerable differences each month. This is especially clear in February and November in panels e and f. Given the large spread in amplitudes for each month, there is enough evidence to proceed with our investigation.

4.1.1. Average Year 12-hr Tide

We can also calculate an average year for our data set, shown in Figure 3. Figures 3a and 3b present the monthly tidal amplitude averaged over the 15 years for the zonal and meridional components, respectively. In the zonal component, we can see that there are two peaks in amplitude in the year, representing the semiannual cycle in tidal amplitudes peaking close to the equinoxes. In April, the first peak reaches amplitudes ~40 m s^{-1} above 95 km, sustaining until mid-May. The second peak occurs in August but with a smaller amplitude of around 24 m s^{-1}. The smallest tidal amplitudes are found near 80 km in height toward the end of March and early April, where tidal amplitudes are near 3 m s^{-1}. In general, examples of larger amplitudes exist between March and September above 90 km, whereas examples of smaller values exist between October and February, especially near 80 km. For the
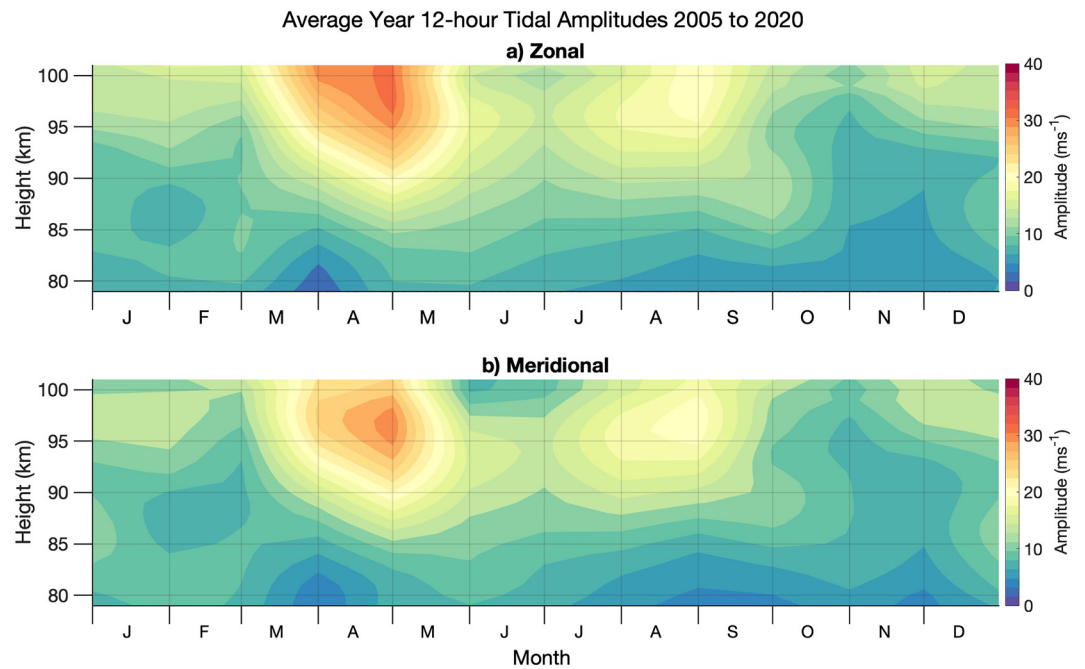
Figure 3. Average year 12-hr tidal amplitudes over the height range 80–100 km for the period 2005–2020 for (a) zonal and (b) meridional components.

meridional component in Figure 3b, the tidal amplitudes display a semiannual cycle with two peaks in amplitude in April and late August. These peaks occur at a similar height and again close to the equinoxes, as in the zonal.

4.2. Correlation of Climate Variables to Interannual Tidal Variability

Next, we explore the result of our linear regression analysis on the 12-hr tidal amplitudes from the meteor radar at Rothera. As we have performed the linear regression analysis on the zonal and meridional components of the 12-hr tide, we have two plots for each index. Here, we present time-height contours of the coefficients from the linear regression analysis for each climate index, as given in Equation 1, e.g., β_1 to β_6. Each result is plotted as a time-height contour plot, with positive values corresponding to an increase in amplitude represented by red shading and negative values corresponding to a decrease in amplitude by blue shading. For each plot, we have overlaid contours representing the significance level using *t*-test statistics (from a two-tailed student's *t*-test), with the dashed contour representing the 80% confidence level and the solid contour indicating the 90% significance level. We will therefore only discuss correlations with 90% significance. In all of the indices used in this study, we use response to suggest a link between the index being studied and the variability of the 12-hr tidal amplitude in the MLT. We note that correlations do not inherently imply causation, we use them here as a guide to the causal mechanisms at play.

We have scaled the color bar axis using the difference between the 90th and 10th percentiles of each index, hereafter defined as the interdecile range, α. Table 1 presents these values for each index. We use α to give a comparable scale for each index so we may compare the relative correlations. As α is calculated using the climate index, it is the same regardless of the tidal component.

4.2.1. Solar Flux

In Figure 4, we present the results for F10.7 solar flux from the linear regression analysis of the 12-hr tidal amplitudes, i.e., the solar coefficient of the linear model β_1. The most noticeable feature in both the zonal (Figure 4a) and the meridional (Figure 4b) is the large negative response at the beginning of

Table 1
The Interdecile Range, α, Used to Scale the Linear Regression Response Plots (Figures 4–8) for Each Given Index

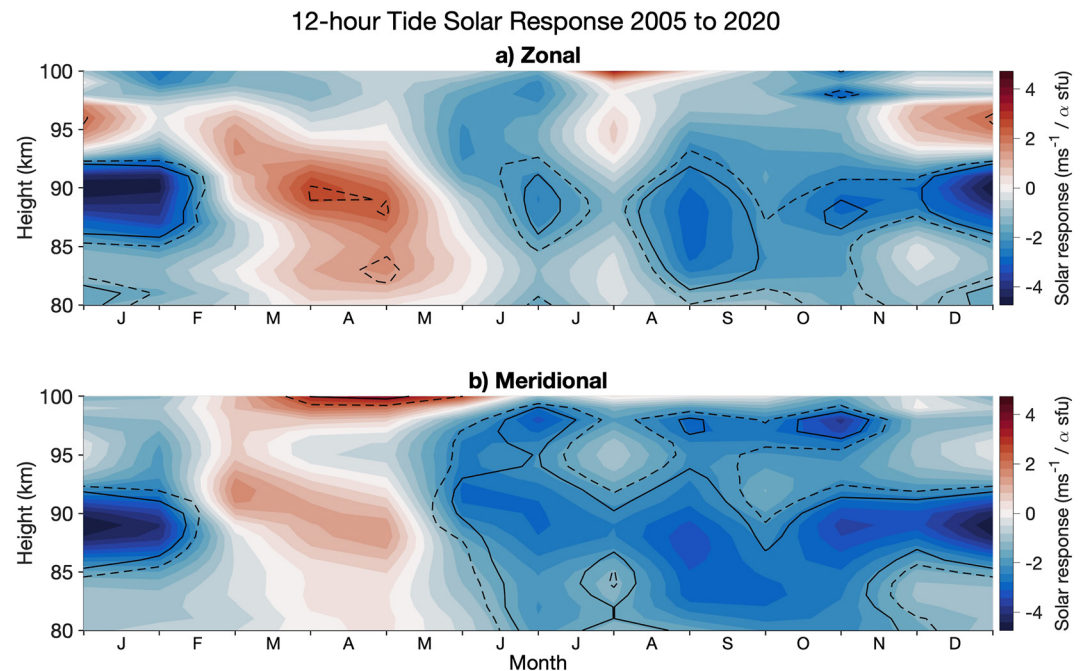| Index	Interdecile range (α)
F10.7 solar flux	57.6 SFU
ENSO	2.67 K
QBO10	45.8 m s^{-1}
QBO30	42.8 m s^{-1}
SAM	4.02 hPa

Figure 4. Twelve-hour tide F10.7 solar flux response to tidal amplitudes over the height range 80–100 km for the period 2005–2020, for the (a) zonal and (b) meridional components. Dashed and solid contours indicate the 80% and 90% confidence intervals, respectively, according to the *t*-test.

the year and at the end of the year, between 85 and 93 km, where we see a response of up to -4 m s^{-1} per α SFU solar flux (where $\alpha = 57.6$ SFU). The meridional component also has a large statistically significant region in mid-June, extending through December and into February at a large range of heights. In the middle of the year, this response is -3 m s^{-1} per α SFU in June at 90 km, growing to -4 m s^{-1} per α SFU at 90 km in December.

4.2.2. ENSO

The results of the response of 12-hr tidal amplitudes above Rothera to ENSO are presented in Figures 5a and 5b in the zonal and meridional components, respectively. ENSO does not present many significant regions compared to the other indices used in this study. The only notable feature in both components is a small significant region below 82 km in height from late February to April with a response of -2 m s^{-1} per α K, where $\alpha = 2.67$ K. As there are not any further significant regions, we are unable to make any further correlations with the 12-hr tide above Rothera.

4.2.3. QBO at 10 hPa

The results for the response of the 12-hr tide to the QBO10 index are presented in Figures 6a and 6b for the zonal and meridional components, respectively. The most striking feature in this figure is a strong negative response of -5 m s^{-1} per α m s^{-1} QBO10 from December to January at most heights (where $\alpha = 45.8$ m s^{-1} QBO10). This feature is also found in the zonal component but is weaker. Both components also have significant responses in the middle of the year. In the zonal component, this is seen from May to June centered at 95 km with a 4 m s^{-1} per α m s^{-1} QBO10 response and in the meridional, we see a -3 m s^{-1} per α m s^{-1} QBO10 response from June to July centered at 95 km.

4.2.4. QBO at 30 hPa

The results for the response of the 12-hr tide to the QBO30 index are presented in Figures 6c and 6d for the zonal and meridional components, respectively. In the zonal component, Figure 6c, there are instances of significance across the year. The most noticeable instance is from May to June, where there is a weak positive response of 3 m s^{-1} per α m s^{-1} QBO30 below 90 km. In November, there is a further significant region beginning at 4 m s^{-1} per α m s^{-1} QBO30 and extending through to January, becoming a negative response of -2 m s^{-1} per α m s^{-1} QBO30. The QBO30 index in the meridional, Figure 6d, exhibits a strong negative response in January of
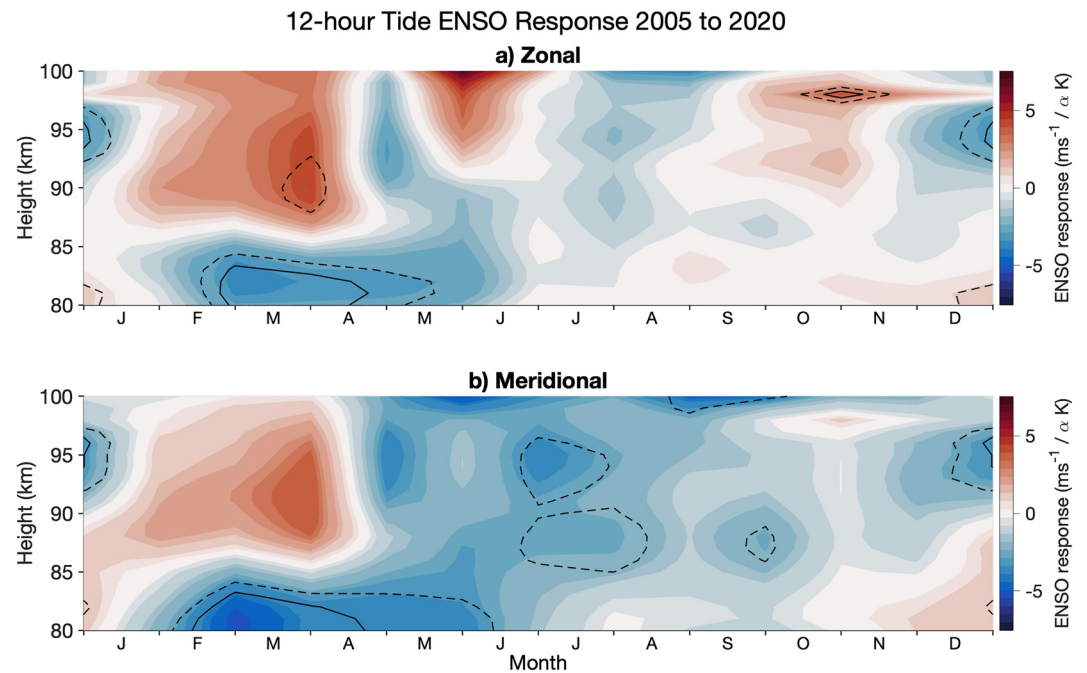
Figure 5. Twelve-hour tide El Niño Southern Oscillation (ENSO) response to tidal amplitudes over the height range 80–100 km for the period 2005–2020, for the (a) zonal and (b) meridional components. Dashed and solid contours indicate the 80% and 90% confidence intervals, respectively, according to the *t*-test.

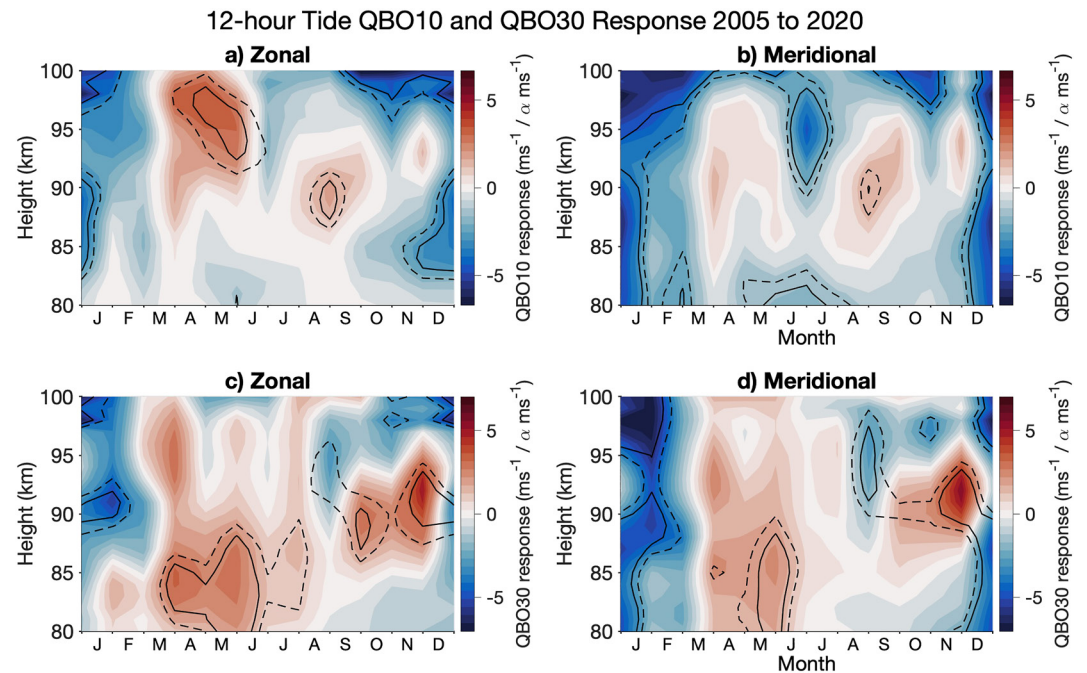
Figure 6. Twelve-hour tide QBO10 and QBO30 response to tidal amplitudes over the height range 80–100 km for the period 2005–2020, for QBO 10 in the (a) zonal and (b) meridional components, respectively, and for QBO30 in the (c) zonal and (d) meridional components, respectively. Dashed and solid contours indicate the 80% and 90% confidence intervals, respectively, according to the *t*-test.
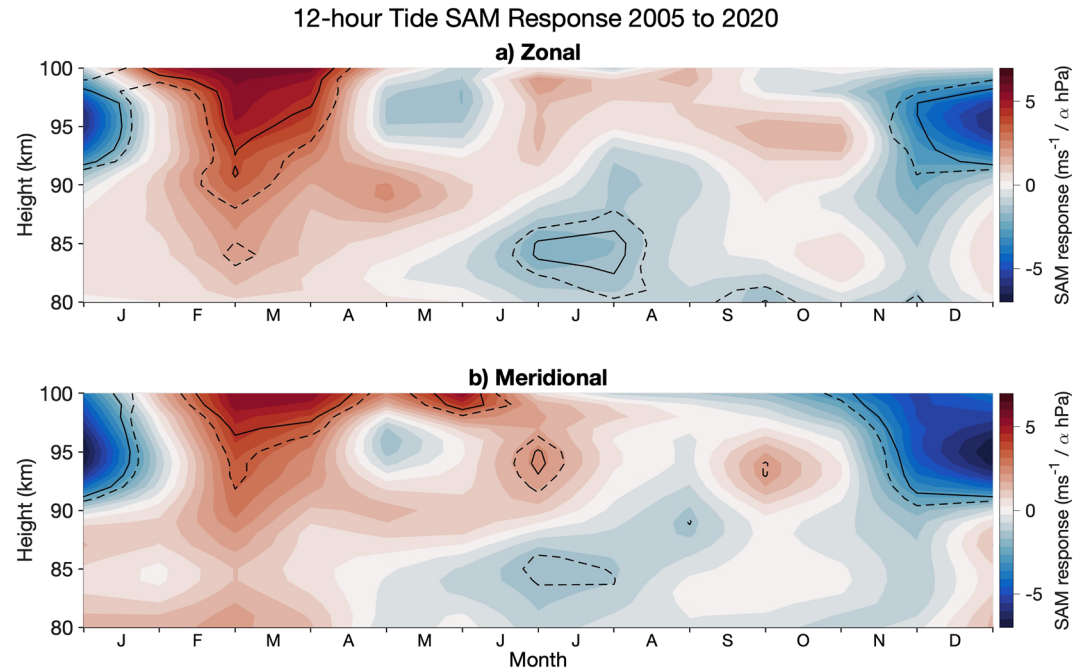
Figure 7. Twelve-hour tide Southern Annular Mode (SAM) response to tidal amplitudes over the height range 80–100 km for the period 2005 to 2020, for the (a) zonal and (b) meridional components. Dashed and solid contours indicate the 80% and 90% confidence intervals, respectively, according to the *t*-test.

-6 m s^{-1} per α m s^{-1} QBO30 above 95 km and -4 m s^{-1} per α m s^{-1} QBO30 below 90 km during January (where $\alpha = 42.8$ m s^{-1}). Unlike QBO10, this feature is not reflected in the zonal component in Figure 6c.

4.2.5. SAM

The results for the response of the 12-hr tide to the SAM index are presented in Figures 7a and 7b for the zonal and meridional components, respectively. In both the zonal and meridional components, there are significant regions from December to January above 90 km. This reaches -5 m s^{-1} per α hPa SAM (where $\alpha = 4.02$ hPa). We also see a positive response in each component from February to April above 95 km. Here, we see responses of 5 m s^{-1} per α hPa SAM. The other regions of significance seen are small and also have a minimal magnitude.

4.2.6. Linear Trends

The results for the presence of linear trends are presented in Figures 8a and 8b for the zonal and meridional components, respectively. There is a large significant response of -1 m s^{-1}/year from February to June above 90 km in the zonal component (Figure 8a). This is a large response when considering our 15 years of data. We also see small contributions in the meridional component in Figure 8b. For example, in late August, above 87 km, there is a response of 0.2 m s^{-1}/year. Over 15 years of our data set, this becomes 3 m s^{-1}. Compared to monthly amplitudes at this time of around 10–15 m s^{-1}, the correlations are not to be ignored.

5. Discussion

5.1. Interannual Variability

Using a meteor radar based at Rothera in the Antarctic, we have observed the seasonal climatology and interannual variability of 12-hr tidal amplitudes in the Antarctic MLT and investigated the correlation of this variability to climate indices representing solar F10.7 flux, ENSO, QBO10, QBO30, and SAM as well as investigating linear trends by performing a linear regression on the 12-hr tidal amplitudes for the period between 2005 and 2020, inclusive. We have found that solar flux, QBO10, QBO30, and SAM all have varying degrees of correlation with the amplitudes of the 12-hr tide, with a linear trend also present above 95 km from January to May. In contrast, we have found minimal correlation between ENSO and the 12-hr tidal amplitudes.
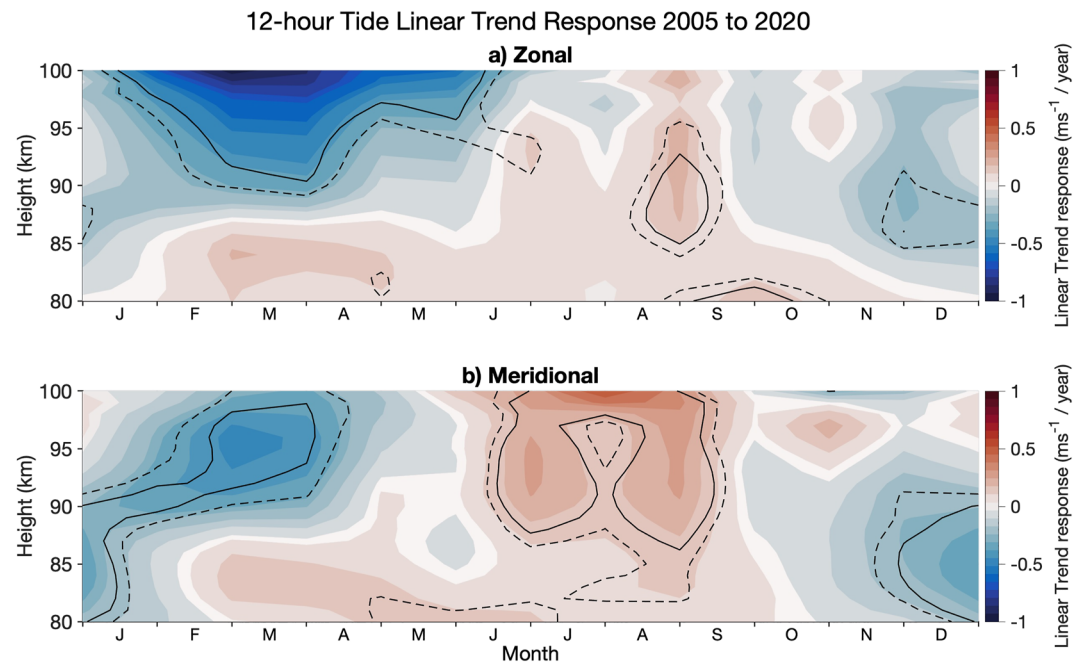
Figure 8. Twelve-hour tide time response to tidal amplitudes over the height range 80–100 km for the period 2005–2020, for the (a) zonal and (b) meridional components. Dashed and solid contours indicate the 80% and 90% confidence intervals, respectively, according to the *t*-test.

In Figure 2, we presented the 12-hr monthly mean tidal amplitudes at 90 and 95 km measured at Rothera. Our analysis reveals a similar seasonal cycle to that reported in other Antarctic studies, with the largest amplitudes occurring in spring and autumn (e.g., Beldon & Mitchell, 2010; Dempsey et al., 2021; Stober, Janches et al., 2021). Further, we found considerable interannual variability in the tidal amplitudes in the MLT. Such variability appears to be a persistent feature of the polar 12-hr tide and has been reported in a number of other studies, including Baumgaertner et al. (2005) and Merzlyakov et al. (2009). Conte et al. (2017) measured the amplitude of the 12-hr tide at Davis (69°S, 78°E) using a meteor radar from 2009 to 2013 and noted less interannual variability in the winter months and more in summer. Moreover, Baumgaertner et al. (2005) found that the seasonal behavior of the 12-hr tide bears a striking resemblance to the behavior of planetary wave activity at polar latitudes. They noted that long-term variations in planetary-wave amplitudes are similar to those of the 12-hr tide and so proposed that planetary waves may therefore modulate the interannual variability of the tide.

Rothera is also host to an MF radar. Hibbins et al. (2007) used data from this MF radar recorded between 1997 and 2005 to calculate MLT tidal amplitudes and phases. Note that they did not investigate interannual variability of the tidal amplitudes. They reported a 12-hr tide with a semiannual cycle in amplitudes, peaking in April and September—as we observe here. However, we observe significantly larger amplitudes at the upper heights with the meteor radar. Further, the tidal amplitudes we present in Figure 2 at 95 km are generally larger than those at 90 km, but this amplitude growth with height is not apparent in the MF-radar observations of Hibbins et al. (2007). For example, our results indicate considerable amplitude increases with increasing height over the height range 90–95 km, e.g., from 22 m s^{-1} in April 2007 to 33 m s^{-1} in April 2008. This is in contrast to the MF-radar observations, which showed approximately constant amplitudes throughout all heights of around 7 m s^{-1} with the amplitudes actually decreasing slightly at heights above about 95 km. Although made in different years, these differences are similar to meteor/MF-radar biases reported elsewhere (Hines et al., 1993; Manson et al., 2004) that have been attributed to properties of the MF radar technique (Wilhelm et al., 2017).

In addition, Conte et al. (2017) measured polar 12-hr tidal amplitudes at Davis (69°S, 78°E) from 2009 to 2013 and found considerable interannual variability, with summer demonstrating the most extensive variability. While they found a seasonal cycle, the timing of this cycle varied with each year. They proposed that the variability seen may be due to migrating and nonmigrating modes, as proposed by Murphy (2003). They found that between December and February, a westward propagating zonal wave number 1 nonmigrating component dominates the

nonmigrating tidal contributions to the 12-hr tide at 68°–69°S and that between April and October, nonmigrating tide activity is very low, so the westward zonal wave number 2 migrating component dominates. Similarly to our study, Conte et al. (2017) could not decompose the tidal amplitudes observed as they used a single station at this latitude.

5.2. Correlations Between Tidal Amplitudes and Climate Indices

We have used a linear regression analysis to investigate possible links between the monthly amplitudes of the Antarctic 12-hr tide in the MLT and a number of climate indices. We have found that solar flux, QBO10, QBO30, and SAM all have at least some heights and times where there are significant correlations, but ENSO does not show a significant correlation. We have also found a significant linear trend in the zonal component of the 12-hr tidal amplitude response.

5.2.1. Solar Flux

In Figure 4, we found correlations at the 90% significance level during summer suggesting a -4 m s^{-1} per α SFU ($\alpha = 57.6$ SFU) relationship in both the zonal and meridional components at heights of 85–93 km from December to mid-February. This significant region begins in mid-June and extends through to the end of the year in the meridional, where the response becomes strong in December. This implies a negative correlation between F10.7 and the 12-hr tidal amplitude. At Antarctic latitudes, Baumgaertner et al. (2005) investigated the relationship between solar flux and 12-hr tidal amplitudes at Scott Base (78°S, 167°E) and found a negative correlation between solar activity and 12-hr tidal amplitudes at 80 km over the time period 1985–2004. Our results thus reinforce the suggestion that 12-hr tidal amplitudes may decrease, at least in some months, during times of high solar activity (F10.7). This negative correlation has also been found at other latitudes (Bremer et al., 1997; Namboothiri et al., 1993).

Nonlinear interactions between tides and planetary waves play a significant role in the behavior of the 12-hr tide, and therefore the relationship to the solar cycle may be in part due to changes in planetary wave activity as a result of changing solar flux (Baumgaertner et al., 2005; Salby & Callaghan, 2004). A change in planetary wave activity could change the generation of migrating tidal modes, which are thought to be forced mainly by nonlinear interactions between tides and planetary waves, generating secondary waves, which include the nonmigrating tidal modes (Beard et al., 1999; Gu & Du, 2018; Palo et al., 2007; Teitelbaum & Vial, 1991).

Also, during the westerly QBO phase, Labitzke (2004) found the intensity of the Antarctic vortex to be inversely associated with solar activity. Thus, they proposed during periods of strong solar activity, a weaker Antarctic vortex begins later in the year and breaks up early, affecting the MLT tides' peak amplitudes. These changes may be seen here; however, measurements of the Antarctic vortex would be required (Baldwin et al., 2001; Hibbins et al., 2009).

5.2.2. ENSO

Following Pedatella and Liu (2012), who concluded that ENSO drives MLT tidal interannual variability, we included ENSO in our linear regression model as a potential driver. However, in Figure 5, we found only a small significant response between the ENSO index and monthly 12-hr tidal amplitudes. Further, at equatorial latitudes, Liu et al. (2017) simulated that a ground-based station located south of the equator would detect a substantial enhancement of the 24-hr tide in the meridional component during both El Niño and La Niña but only during El Niño in the zonal component and temperature. Consequently, there may only be an enhancement of the 24-hr tide by ENSO and potentially a reason why limited significant correlations are found. Our region of significance coincided with only a small response. Therefore, we can conclude that ENSO shows no extensive significant correlation with monthly tidal amplitudes.

5.2.3. QBO

For both the QBO10 and QBO30 indices, Figure 6, we have seen significant correlations. These have been more prominent in the meridional component in the summertime, where we have seen correlations of -5 m s^{-1} per α m s^{-1} QBO10. Ford et al. (2009) investigated mesospheric winds and the polar vortex above Halley, Antarctica (76°S, 27°W) and found winds are modulated by the action of the equatorial QBO on planetary wave propagation. They hypothesized interaction of the QBO with gravity waves and planetary waves generates QBO-like effects

in the mesosphere. If this QBO enhancement were westerly in the northern hemisphere in winter, it would allow gravity waves to cross into the southern hemisphere, reducing planetary wave activity in the southern hemisphere and consequently reducing nonmigrating tidal amplitudes.

Between 1996 and 2004, Hibbins et al. (2007) reported a clear and substantial QBO dependence on the 12-hr tide measured at Halley (76°S, 27°W) with meteor winds from the SuperDARN radar. The effect was shown to be strongest during the summer months, with a 2 m s^{-1} decrease in amplitude when the QBO at 35 hPa was positive and a similar rise in amplitude when the QBO at 5 hPa was positive. These findings are consistent as the phase of the QBO changes with increasing equatorial altitude, with the phase of the QBO recorded at 35 hPa being opposite that of the QBO measured at 5 hPa (Baldwin & Dunkerton, 1998). For this reason, we used two QBO indices, one at 10 hPa and one at 30 hPa. We have also found a negative correlation during the summer months, especially true in the meridional components of the QBO10 and QBO30 tidal amplitude response.

Further, Hibbins et al. (2010) used 12 years of horizontal wind data from the Scott Base MF radar and the Halley SuperDARN radar measured between January 1996 and December 2007 to investigate the migrating ($S = 2$) and nonmigrating ($S = 1$) components of the 12-hr tide around 78°S. They found the amplitude of the summer time $S = 1$ component of the tide shows a large interannual fluctuation, and a quasi-biennial periodicity is observed out of phase with the equatorial QBO recorded at 30 hPa. The amplitude and phase of the migrating $S = 2$ component of the tide show no significant QBO relationship, implying that the previously found QBO dependency on the summertime 12-hr tide at Halley is only driven by the nonmigrating $S = 1$ component.

5.2.4. SAM

We have found that above heights of 90 km, there is a significant correlation from mid-February to mid-April with a positive response of 5 m s^{-1} per α hPa (where $\alpha = 4.02$ hPa). There is then a period of negative response from mid-November to mid-January with a -5 m s^{-1} per α hPa. The positive response we have observed occurs during austral spring. Fogt and Marshall (2020) suggested that zonal wind anomalies during austral spring often extend into the stratosphere and become stronger with height. Hence, an enhancement of zonal wind anomalies in the 12-hr tide source region may influence the tidal amplitudes in the MLT, possibly resulting in the enhancement of tidal amplitudes presented in Figure 7.

In contrast, Merzlyakov et al. (2009) sought to identify any correlations between the SAM index and MLT winds and tides and did not find any correlation. They used a meteor radar located at Molodezhnaya (67.7°S, 45.9°E) and MF radars at Mawson (67.6°S, 62.9°E) and Davis (68.6°S, 78.0°E). However, in the current study, we employ a meteor radar with height finding rather than a radar without like that used by Merzlyakov et al. (2009). A system without height finding is unable to determine the growth with height of the tidal amplitudes present in the MLT. Therefore, they observe the average and will miss elements of the tidal amplitude structure. Also, MF radars are known to underestimate tidal amplitudes at the upper heights. In combination, this means that in our study, we have been able to use the height finding to our advantage to find a correlation.

5.2.5. Linear Trends

We have found a significant negative correlation above 95 km from January to May in the zonal component of the tides when investigating linear trends. This suggests that the tidal amplitudes are decreasing with time at this height and period of the year. As mentioned previously, Baumgaertner et al. (2005) found a positive trend in tidal amplitudes and suggested this was due to a rise in atmospheric CO_2 levels causing cooling, resulting in density decreasing more rapidly with height. This would lead to a larger increase of tidal amplitudes with height. This is not something that we observe in the present study. We observe the strongest linear trend at the upper heights, indicating that the tidal amplitudes are not growing to the same extent year on year.

6. Conclusions

In this study, we have investigated the interannual variability of the tidal amplitudes using linear regression analysis to identify any links between climate indices and the 12-hr tidal amplitudes in the zonal and meridional components. This study has used a 15-year-long data set of 12-hr tidal amplitudes from a meteor radar located at the British Antarctic Survey base at Rothera (68°S, 68°W). We have shown that the considerable interannual variability of the amplitude of the 12-hr tide above Rothera is correlated with several climate indices, specifically

ENSO, QBO10, QBO30, and SAM. This implies linear connections between the 12-hr tide in the Antarctic and atmospheric phenomena at other latitudes and heights.

We conclude that

1. We observe persistent large-amplitude 12-hr tidal amplitudes throughout the period 2005–2020 at Rothera, with monthly mean values reaching 13.0 m s^{-1} in spring, 12.0 m s^{-1} in summer, 21.2 m s^{-1} in autumn, and 16.4 m s^{-1} in winter.
2. The 12-hr monthly mean tidal amplitudes show significant interannual variability. For example, for 95 km, the 2σ range in monthly mean 12-hr tidal amplitudes is 13.4 m s^{-1} in spring, 11.2 m s^{-1} in summer, 18.6 m s^{-1} in autumn, and 7.0 m s^{-1} in winter.
3. The climatological tidal amplitudes we observe are larger than those observed using MF radars at similar latitudes. We propose these differences are due to MF radar bias at the upper heights.
4. Using linear regression analysis, we find that F10.7 solar flux has a significant negative correlation between tidal amplitudes in both the zonal and meridional components. This is from December to February in both components, with the meridional component showing an additional response from June to November. This strong response has a magnitude of -4 m s^{-1} per α SFU, where $\alpha = 57.6$ SFU.
5. We find that both the QBO10 and QBO30 indices show linear correlations between the 12-hr tidal amplitudes of the MLT. There is a strong negative correlation in the meridional component of the tidal amplitude response of the QBO10 and QBO30 result, with strong responses present in summer at all heights, with the upper heights having a response of -5 m s^{-1} per α m s^{-1} QBO10 ($\alpha = 45.8$ m s^{-1} QBO10) and -6 m s^{-1} per α m s^{-1} QBO30 ($\alpha = 42.8$ m s^{-1} QBO30) for the QBO10 and QBO30 indices respectively.
6. The variation of tidal amplitudes with ENSO is much less significant than the other indices, suggesting that there is no linear link between ENSO and Antarctic MLT 12-hr tidal amplitudes.
7. We have identified linear correlations between the SAM and 12-hr monthly tidal amplitudes above Rothera. We see a positive correlation above 95 km from February to April, whereas we see a negative correlation in November and December above 95 km. Both are more apparent in the meridional component.
8. We find that a linear trend is also present in the zonal component of polar 12-hr tidal amplitude response above 95 km between January and May with a response of -1 m s^{-1}/year.

Further investigation is needed to understand the mechanisms behind these potential connections.

Data Availability Statement

The meteor radar data used in this study are from Mitchell, N. (2019): University of Bath: Rothera Skiymet Meteor Radar data (2005-present). Centre for Environmental Data Analysis, 2022. https://catalogue.ceda.ac.uk/uuid/aa44e02718fd4ba49cefe36d884c6e50. The 10.7 cm solar flux data are provided as a service by the National Research Council of Canada https://www.spaceweather.ca/forecast-prevision/solar-solaire/solarflux/sx-5-en.php.

References

Abram, N. J., Mulvaney, R., Vimeux, F., Phipps, S. J., Turner, J., & England, M. H. (2014). Evolution of the southern annular mode during the past millennium. *Nature Climate Change*, *4*(7), 564–569. https://doi.org/10.1038/nclimate2235

Baldwin, M. P., & Dunkerton, T. J. (1998). Quasi-biennial modulation of the southern hemisphere stratospheric polar vortex. *Geophysical Research Letters*, *25*(17), 3343–3346. https://doi.org/10.1029/98GL02445

Baldwin, M. P., Gray, L. J., Dunkerton, T. J., Hamilton, K., Haynes, P. H., Randel, W. J., et al. (2001). The quasi-biennial oscillation. *Reviews of Geophysics*, *39*(2), 179–229. https://doi.org/10.1029/1999RG000073

Baumgaertner, A., McDonald, A., Fraser, G., & Plank, G. (2005). Long-term observations of mean winds and tides in the upper mesosphere and lower thermosphere above Scott Base, Antarctica. *Journal of Atmospheric and Solar-Terrestrial Physics*, *67*(16), 1480–1496. https://doi.org/10.1016/j.jastp.2005.07.018

Beard, A., Mitchell, N., Williams, P., & Kunitake, M. (1999). Non-linear interactions between tides and planetary waves resulting in periodic tidal variability. *Journal of Atmospheric and Solar-Terrestrial Physics*, *61*(5), 363–376. https://doi.org/10.1016/s1364-6826(99)00003-6

Beldon, C., & Mitchell, N. (2009). Gravity waves in the mesopause region observed by meteor radar, 2: Climatologies of gravity waves in the Antarctic and Arctic. *Journal of Atmospheric and Solar-Terrestrial Physics*, *71*(8–9), 875–884. https://doi.org/10.1016/j.jastp.2009.03.009

Beldon, C., Muller, H., & Mitchell, N. (2006). The 8-hour tide in the mesosphere and lower thermosphere over the UK, 1988–2004. *Journal of Atmospheric and Solar-Terrestrial Physics*, *68*(6), 655–668. https://doi.org/10.1016/j.jastp.2005.10.004

Beldon, C. L., & Mitchell, N. J. (2010). Gravity wave-tidal interactions in the mesosphere and lower thermosphere over Rothera, Antarctica (68°S, 68°W). *Journal of Geophysical Research*, *115*, D18101. https://doi.org/10.1029/2009JD013617

Bremer, J., Schminder, R., Greisiger, K., Hoffmann, P., Kürschner, D., & Singer, W. (1997). Solar cycle dependence and long-term trends in the wind field of the mesosphere/lower thermosphere. *Journal of Atmospheric and Solar-Terrestrial Physics*, *59*(5), 497–509. https://doi.org/10.1016/s1364-6826(96)00032-6

Chapman, S., & Lindzen, R. S. (1970). *Atmospheric tides* (1970th ed.). Springer.

Chiodo, G., Marsh, D. R., Garcia-Herrera, R., Calvo, N., & García, J. A. (2014). On the detection of the solar signal in the tropical stratosphere. *Atmospheric Chemistry and Physics*, *14*(11), 5251–5269. https://doi.org/10.5194/acp-14-5251-2014

Conte, J. F., Chau, J. L., Stober, G., Pedatella, N., Maute, A., Hoffmann, P., et al. (2017). Climatology of semidiurnal lunar and solar tides at middle and high latitudes: Interhemispheric comparison. *Journal of Geophysical Research: Space Physics*, *122*, 7750–7760. https://doi.org/10.1002/2017JA024396

Davis, R. N., Du, J., Smith, A. K., Ward, W. E., & Mitchell, N. J. (2013). The diurnal and semidiurnal tides over Ascension Island (°S, 14°W) and their interaction with the stratospheric quasi-biennial oscillation: Studies with meteor radar, eCMAM and WACCM. *Atmospheric Chemistry and Physics*, *13*(18), 9543–9564. https://doi.org/10.5194/acp-13-9543-2013

Day, K. A., Taylor, M. J., & Mitchell, N. J. (2012). Mean winds, temperatures and the 16- and 5-day planetary waves in the mesosphere and lower thermosphere over bear lake observatory (42°N, 111°W). *Atmospheric Chemistry and Physics*, *12*(3), 1571–1585. https://doi.org/10.5194/acp-12-1571-2012

Dempsey, S. M., Hindley, N. P., Moffat-Griffin, T., Wright, C. J., Smith, A. K., Du, J., & Mitchell, N. J. (2021). Winds and tides of the Antarctic mesosphere and lower thermosphere: One year of meteor-radar observations over Rothera (68°S, 68°W) and comparisons with WACCM and eCMAM. *Journal of Atmospheric and Solar-Terrestrial Physics*, *212*, 105510. https://doi.org/10.1016/j.jastp.2020.105510

Dhadly, M. S., Emmert, J. T., Drob, D. P., McCormack, J. P., & Niciejewski, R. J. (2018). Short-term and interannual variations of migrating diurnal and semidiurnal tides in the mesosphere and lower thermosphere. *Journal of Geophysical Research: Space Physics*, *123*, 7106–7123. https://doi.org/10.1029/2018JA025748

Fiedler, J., Baumgarten, G., & von Cossart, G. (2005). Mean diurnal variations of noctilucent clouds during 7 years of lidar observations at ALOMAR. *Annales Geophysicae*, *23*(4), 1175–1181. https://doi.org/10.5194/angeo-23-1175-2005

Fogt, R. L., & Marshall, G. J. (2020). The southern annular mode: Variability, trends, and climate impacts across the southern hemisphere. *WIREs Climate Change*, *11*(4), e652. https://doi.org/10.1002/wcc.652

Forbes, J. M., Zhang, X., Palo, S., Russell, J., Mertens, C. J., & Mlynczak, M. (2008). Tidal variability in the ionospheric dynamo region. *Journal of Geophysical Research*, *113*, A02310. https://doi.org/10.1029/2007JA012737

Ford, E. A. K., Hibbins, R. E., & Jarvis, M. J. (2009). QBO effects on Antarctic mesospheric winds and polar vortex dynamics. *Geophysical Research Letters*, *36*, L20801. https://doi.org/10.1029/2009GL039848

Fritts, D. C., & Alexander, M. J. (2003). Gravity wave dynamics and effects in the middle atmosphere. *Reviews of Geophysics*, *41*(1), 1003. https://doi.org/10.1029/2001RG000106

Gan, Q., Du, J., Fomichev, V. I., Ward, W. E., Beagley, S. R., Zhang, S., & Yue, J. (2017). Temperature responses to the 11 year solar cycle in the mesosphere from the 31 year (1979–2010) extended Canadian middle atmosphere model simulations and a comparison with the 14 year (2002–2015) TIMED/SABER observations. *Journal of Geophysical Research: Space Physics*, *122*, 4801–4818. https://doi.org/10.1002/2016JA023564

Gu, H., & Du, J. (2018). On the roles of advection and solar heating in seasonal variation of the migrating diurnal tide in the stratosphere, mesosphere, and lower thermosphere. *Atmosphere*, *9*(11), 440. https://doi.org/10.3390/atmos9110440

Guharay, A., Batista, P., & Andrioli, V. (2019). Investigation of solar cycle dependence of the tides in the low latitude MLT using meteor radar observations. *Journal of Atmospheric and Solar-Terrestrial Physics*, *193*, 105083. https://doi.org/10.1016/j.jastp.2019.105083

Hagan, M. E., & Forbes, J. M. (2002). Migrating and nonmigrating diurnal tides in the middle and upper atmosphere excited by tropospheric latent heat release. *Journal of Geophysical Research*, *107*(D24), 4754. https://doi.org/10.1029/2001JD001236

Hibbins, R., Espy, P., Jarvis, M., Riggin, D., & Fritts, D. (2007). A climatology of tides and gravity wave variance in the MLT above Rothera, Antarctica obtained by MF radar. *Journal of Atmospheric and Solar-Terrestrial Physics*, *69*(4–5), 578–588. https://doi.org/10.1016/j.jastp.2006.10.009

Hibbins, R., Marsh, O., McDonald, A., & Jarvis, M. (2010). Interannual variability of the s=1 and s=2 components of the semidiurnal tide in the Antarctic MLT. *Journal of Atmospheric and Solar-Terrestrial Physics*, *72*(9–10), 794–800. https://doi.org/10.1016/j.jastp.2010.03.026

Hibbins, R. E., Jarvis, M. J., & Ford, E. A. K. (2009). Quasi-biennial oscillation influence on long-period planetary waves in the Antarctic upper mesosphere. *Journal of Geophysical Research*, *114*, D09109. https://doi.org/10.1029/2008JD011174

Hindley, N. P., Cobbett, N., Fritts, D. C., Janchez, D., Mitchell, N. J., Moffat-Griffin, T., et al. (2021). Radar observations of winds, waves and tides in the mesosphere and lower thermosphere over south Georgia Island (54°S, 36°W) and comparison to WACCM simulations. *Atmospheric Chemistry and Physics*, *22*, 9435–9459. https://doi.org/10.5194/acp-2021-981

Hines, C., Adams, G., Brosnahan, J., Djuth, F., Sulzer, M., Tepley, C., & Baelen, J. V. (1993). Multi-instrument observations of mesospheric motions over Arecibo: Comparisons and interpretations. *Journal of Atmospheric and Terrestrial Physics*, *55*(3), 241–287. https://doi.org/10.1016/0021-9169(93)90069-b

Hocking, W., Fuller, B., & Vandepeer, B. (2001). Real-time determination of meteor-related parameters utilizing modern digital technology. *Journal of Atmospheric and Solar-Terrestrial Physics*, *63*(2–3), 155–169. https://doi.org/10.1016/s1364-6826(00)00138-3

Kalnins, A. (2018). Multicollinearity: How common factors cause type 1 errors in multivariate regression. *Strategic Management Journal*, *39*(8), 2362–2385. https://doi.org/10.1002/smj.2783

Kumari, K., & Oberheide, J. (2020). QBO, ENSO, and solar cycle effects in short-term nonmigrating tidal variability on planetary wave timescales from SABER—An information-theoretic approach. *Journal of Geophysical Research: Atmospheres*, *125*, e2019JD031910. https://doi.org/10.1029/2019JD031910

Labitzke, K. (2004). On the signal of the 11-year sunspot cycle in the stratosphere and its modulation by the quasi-biennial oscillation. *Journal of Atmospheric and Solar-Terrestrial Physics*, *66*(13–14), 1151–1157. https://doi.org/10.1016/j.jastp.2004.05.011

Laskar, F. I., Chau, J. L., Stober, G., Hoffmann, P., Hall, C. M., & Tsutsumi, M. (2016). Quasi-biennial oscillation modulation of the middle- and high-latitude mesospheric semidiurnal tides during August-September. *Journal of Geophysical Research: Space Physics*, *121*, 4869–4879. https://doi.org/10.1002/2015JA022065

Lee, D. Y., Petersen, M. R., & Lin, W. (2019). The southern annular mode and Southern Ocean surface westerly winds in E3SM. *Earth and Space Science*, *6*, 2624–2643. https://doi.org/10.1029/2019EA000663

Lieberman, R. S., Riggin, D. M., Ortland, D. A., Nesbitt, S. W., & Vincent, R. A. (2007). Variability of mesospheric diurnal tides and tropospheric diurnal heating during 1997–1998. *Journal of Geophysical Research*, *112*, D20110. https://doi.org/10.1029/2007JD008578

Liu, H., Sun, Y.-Y., Miyoshi, Y., & Jin, H. (2017). ENSO effects on MLT diurnal tides: A 21 year reanalysis data-driven GAIA model simulation. *Journal of Geophysical Research: Space Physics*, *122*, 5539–5549. https://doi.org/10.1002/2017JA024011

Liu, H.-L. (2016). Variability and predictability of the space environment as related to lower atmosphere forcing. *Space Weather*, *14*, 634–658. https://doi.org/10.1002/2016SW001450

Manson, A. H., Meek, C. E., Hall, C. M., Nozawa, S., Mitchell, N. J., Pancheva, D., et al. (2004). Mesopause dynamics from the scandinavian triangle of radars within the PSMOS-DATAR project. *Annales Geophysicae*, *22*(2), 367–386. https://doi.org/10.5194/angeo-22-367-2004

Marshall, G. J. (2003). Trends in the southern annular mode from observations and reanalyses. *Journal of Climate*, *16*(24), 4134–4143. https://doi.org/10.1175/1520-0442(2003)016<4134:titsam>2.0.co;2

Marshall, G. J. (2018). Marshall southern annular mode (SAM) index (station-based). Retrieved from https://climatedataguide.ucar.edu/climate-data/marshall-southern-annular-mode-sam-index-station-based

Merzlyakov, E., Murphy, D., Vincent, R., & Portnyagin, Y. (2009). Long-term tendencies in the MLT prevailing winds and tides over Antarctica as observed by radars at Molodezhnaya, Mawson and Davis. *Journal of Atmospheric and Solar-Terrestrial Physics*, *71*(1), 21–32. https://doi.org/10.1016/j.jastp.2008.09.024

Mitchell, N., & Beldon, C. (2009). Gravity waves in the mesopause region observed by meteor radar: 1. A simple measurement technique. *Journal of Atmospheric and Solar-Terrestrial Physics*, *71*(8–9), 866–874. https://doi.org/10.1016/j.jastp.2009.03.011

Mitchell, N. J. (2002). Mean winds and tides in the Arctic mesosphere and lower thermosphere. *Journal of Geophysical Research*, *107*(A1), 1004. https://doi.org/10.1029/2001JA900127

Mthembu, S., Sivakumar, V., Mitchell, N., & Malinga, S. (2013). Studies on planetary waves and tide interaction in the mesosphere/lower thermosphere region using meteor RADAR data from Rothera (68°S, 68°W), Antarctica. *Journal of Atmospheric and Solar-Terrestrial Physics*, *102*, 59–70. https://doi.org/10.1016/j.jastp.2013.04.012

Murphy, D. J. (2003). Observations of a nonmigrating component of the semidiurnal tide over Antarctica. *Journal of Geophysical Research*, *108*(D8), 4241. https://doi.org/10.1029/2002JD003077

Namboothiri, S., Manson, A., & Meek, C. (1993). Variations of mean winds and tides in the upper middle atmosphere over a solar cycle, saskatoon, Canada, 52°n, 107°w. *Journal of Atmospheric and Terrestrial Physics*, *55*(10), 1325–1334. https://doi.org/10.1016/0021-9169(93)90101-4

Nischal, N., Oberheide, J., Mlynczak, M. G., Marsh, D. R., & Gan, Q. (2019). Solar cycle variability of nonmigrating tides in the 5.3 and 15 μm infrared cooling of the thermosphere (100 – 150 km) from SABER. *Journal of Geophysical Research: Space Physics*, *124*, 2338–2356. https://doi.org/10.1029/2018JA026356

Noble, P., Hindley, N., Wright, C., Cullens, C., England, S., Pedatella, N., et al. (2022). Interannual variability of winds in the Antarctic mesosphere and lower thermosphere over Rothera (67°S, 68°W) in radar observations and WACCM-X. *Atmospheric Chemistry and Physics*. https://doi.org/10.5194/acp-2022-150

Palo, S. E., Forbes, J. M., Zhang, X., Russell, J. M., & Mlynczak, M. G. (2007). An eastward propagating two-day wave: Evidence for nonlinear planetary wave and tidal coupling in the mesosphere and lower thermosphere. *Geophysical Research Letters*, *34*, L07807. https://doi.org/10.1029/2006GL027728

Pancheva, D., Mitchell, N., Middleton, H., & Muller, H. (2003). Variability of the semidiurnal tide due to fluctuations in solar activity and total ozone. *Journal of Atmospheric and Solar-Terrestrial Physics*, *65*(1), 1–19. https://doi.org/10.1016/s1364-6826(02)00084-6

Pancheva, D., Mukhtarov, P., & Andonov, B. (2009). Global structure, seasonal and interannual variability of the migrating semidiurnal tide seen in the SABER/TIMED temperatures (2002–2007). *Annales Geophysicae*, *27*(2), 687–703. https://doi.org/10.5194/angeo-27-687-2009

Pedatella, N. M., & Liu, H.-L. (2012). Tidal variability in the mesosphere and lower thermosphere due to the El Niño-Southern Oscillation. *Geophysical Research Letters*, *39*, L19802. https://doi.org/10.1029/2012GL053383

Ramesh, K., Smith, A. K., Garcia, R. R., Marsh, D. R., Sridharan, S., & Kumar, K. K. (2020). Long-term variability and tendencies in migrating diurnal tide from WACCM6 simulations during 1850–2014. *Journal of Geophysical Research: Atmospheres*, *125*, e2020JD033644. https://doi.org/10.1029/2020JD033644

Salby, M., & Callaghan, P. (2004). Evidence of the solar cycle in the general circulation of the stratosphere. *Journal of Climate*, *17*(1), 34–46. https://doi.org/10.1175/1520-0442(2004)017<0034:eotsci>2.0.co;2

Sandford, D., Mitchell, N., Vincent, R., & Murphy, D. (2007). The lunar tides in the Antarctic mesosphere and lower thermosphere. *Journal of Atmospheric and Solar-Terrestrial Physics*, *69*(17–18), 2219–2237. https://doi.org/10.1016/j.jastp.2007.04.010

Sandford, D. J., Beldon, C. L., Hibbins, R. E., & Mitchell, N. J. (2010). Dynamics of the Antarctic and Arctic mesosphere and lower thermosphere—Part 1: Mean winds. *Atmospheric Chemistry and Physics*, *10*(21), 10273–10289. https://doi.org/10.5194/acp-10-10273-2010

Sassi, F. (2004). Effect of El Niño-Southern Oscillation on the dynamical, thermal, and chemical structure of the middle atmosphere. *Journal of Geophysical Research*, *109*, D17108. https://doi.org/10.1029/2003JD004434

Smith, A. K. (2012). Global dynamics of the MLT. *Surveys in Geophysics*, *33*(6), 1177–1230. https://doi.org/10.1007/s10712-012-9196-9

Sobhkhiz-Miandehi, S., Yamazaki, Y., Arras, C., Miyoshi, Y., & Shinagawa, H. (2022). Comparison of the tidal signatures in sporadic e and vertical ion convergence rate, using FORMOSAT-3/COSMIC radio occultation observations and GAIA model. *Earth Planets and Space*, *74*(1), 88. https://doi.org/10.1186/s40623-022-01637-y

Song, B.-G., Song, I.-S., Chun, H.-Y., Lee, C., Kam, H., Kim, Y. H., et al. (2021). Activities of small-scale gravity waves in the upper mesosphere observed from meteor radar at King Sejong station, Antarctica (62.22°S, 58.78°W) and their potential sources. *Journal of Geophysical Research: Atmospheres*, *126*, e2021JD034528. https://doi.org/10.1029/2021JD034528

Sprenger, K., & Schminder, R. (1969). Solar cycle dependence of winds in the lower ionosphere. *Journal of Atmospheric and Terrestrial Physics*, *31*(1), 217–221. https://doi.org/10.1016/0021-9169(69)90100-7

Stober, G., Janches, D., Matthias, V., Fritts, D., Marino, J., Moffat-Griffin, T., et al. (2021). Seasonal evolution of winds, atmospheric tides, and Reynolds stress components in the southern hemisphere mesosphere-lower thermosphere in 2019. *Annales Geophysicae*, *39*(1), 1–29. https://doi.org/10.5194/angeo-39-1-2021

Stober, G., Kuchar, A., Pokhotelov, D., Liu, H., Liu, H.-L., Schmidt, H., et al. (2021). Interhemispheric differences of mesosphere-lower thermosphere winds and tides investigated from three whole-atmosphere models and meteor radar observations. *Atmospheric Chemistry and Physics*, *21*(18), 13855–13902. https://doi.org/10.5194/acp-21-13855-2021

Sundararajan, S. (2020). Equatorial upper mesospheric mean winds and tidal response to strong El Niño and La Niña. *Journal of Atmospheric and Solar-Terrestrial Physics*, *202*, 105270. https://doi.org/10.1016/j.jastp.2020.105270

Teitelbaum, H., & Vial, F. (1991). On tidal variability induced by nonlinear interaction with planetary waves. *Journal of Geophysical Research*, *96*(A8), 14169–14178. https://doi.org/10.1029/91JA01019

Trenberth, K. (2018). Nino SST indices (nino 1 2, 3, 3.4, 4; ONI and TNI). *National Center for Atmospheric Research*. Retrieved from https://climatedataguide.ucar.edu/climate-data/nino-sst-indices-nino-12-3-34-4-oni-and-tni

Trenberth, K. E. (2002). Evolution of El Niño-Southern Oscillation and global atmospheric surface temperatures. *Journal of Geophysical Research*, *107*(D8), 4065. https://doi.org/10.1029/2000JD000298

Vadas, S. L., Liu, H.-L., & Lieberman, R. S. (2014). Numerical modeling of the global changes to the thermosphere and ionosphere from the dissipation of gravity waves from deep convection. *Journal of Geophysical Research: Space Physics*, *119*, 7762–7793. https://doi.org/10.1002/2014JA020280

Vitharana, A., Zhu, X., Du, J., Oberheide, J., & Ward, W. E. (2019). Statistical modeling of tidal weather in the mesosphere and lower thermosphere. *Journal of Geophysical Research: Atmospheres*, *124*, 9011–9027. https://doi.org/10.1029/2019JD030573

Webster, A. (2012). *Introductory regression analysis: With computer application for business and economics*. Taylor & Francis Group.

Wilhelm, S., Stober, G., & Chau, J. L. (2017). A comparison of 11-year mesospheric and lower thermospheric winds determined by meteor and MF radar at 69 N. *Annales Geophysicae*, *35*(4), 893–906. https://doi.org/10.5194/angeo-35-893-2017

Yiğit, E., & Medvedev, A. S. (2015). Internal wave coupling processes in earth's atmosphere. *Advances in Space Research*, *55*(4), 983–1003. https://doi.org/10.1016/j.asr.2014.11.020

Yiğit, E., Medvedev, A. S., & Ern, M. (2021). Effects of latitude-dependent gravity wave source variations on the middle and upper atmosphere. *Frontiers in Astronomy and Space Sciences*, *7*, 614018. https://doi.org/10.3389/fspas.2020.614018